Eur. Phys. J. B **15**, 357–369 (2000)

THE EUROPEAN PHYSICAL JOURNAL B

EDP Sciences

Improved modeling of flows down inclined planes

C. Ruyer-Quil and P. Manneville[a]

Laboratoire d'Hydrodynamique, CNRS UMR 7646, École Polytechnique, 91128 Palaiseau, France

Received 14 September 1999 and Received in final form 6 January 2000

Abstract. New models of film flows down inclined planes have been derived by combining a gradient expansion at first or second order to weighted residual techniques with polynomials as test functions. The two-dimensional formulation has been extended to account for three-dimensional flows as well. The full second-order two-dimensional model can be expressed as a set of four coupled evolution equations for four slowly varying fields, the thickness h, the flow rate q and two other quantities measuring the departure from the flat-film semi-parabolic velocity profile. A simplified model has been obtained in terms of h and q only. Including viscous dispersion effects properly, it closely sticks to the asymptotic expansion in the appropriate limit. Our new models improve over previous ones in that they remain valid deep into the strongly nonlinear regime, as shown by the comparison of our results relative to travelling-wave and solitary-wave solutions with those of both direct numerical simulations and experiments.

PACS. 47.20.Ma Interfacial instability – 47.20.Ky Nonlinearity (including bifurcation theory)

1 Introduction

Film flows down inclined planes [1,2] are of special interest in the study of pattern formation and the transition to space-time chaos. In particular, they belong to the class of open flows and, as such are expected to bring novel features [3] when compared to closed extended systems, typically convecting systems, to which many studies have been devoted [4].

Physically speaking, the problem is well posed. A trivial solution to the Navier-Stokes equations, serving as basic flow, is easily found in the form of a steady uniform parallel flow with parabolic velocity profile, often called Nusselt's solution. Thin films over sufficiently steep surfaces turn out to be unstable against long wavelength infinitesimal perturbations, *i.e.* with wavelengths large when compared to the thickness of the flow, the dynamics of which is essentially controlled by viscosity and surface tension effects. Close to the threshold these waves present themselves as streamwise surface undulations free of spanwise modulations ("two-dimensional" waves) emerging from a supercritical (*i.e.* continuous) bifurcation. Farther from threshold, they saturate at finite amplitudes and, depending on control parameters, may develop secondary instabilities involving spanwise modulations ("three-dimensional" instabilities) or first evolve into localized "solitary" structures that subsequently destabilize [5] up to developed space-time chaos.

The theoretical understanding of the problem starting directly from the full Navier-Stokes (NS) seeming out to reach, one might hope some enlightening from their numerical investigation. However this remains a difficult task owing to the presence of a free boundary, so that the two-dimensional case is the only one to be reliably implemented [6,7]. In the same vein, realistic results can be obtained [8] from a simplification of the NS equations within the framework of the so-called boundary layer (BL) approximation incorporating the condition that streamwise gradients are small when compared to cross-stream variations [9], but one is left with a problem that has the same space dimensionality as the original one. At any rate, the numerical approach, even restricted to the two-dimensional case, does not give much insight into the instability and pattern-formation mechanisms. The derivation of reliable simplified models retaining the most relevant physical features of the problem would thus be an important step towards the understanding of the nonlinear development of waves in transitional film flows.

As a matter of fact, many models have been derived since the pioneering work of Kapitza [10]. On general grounds, the first step in any modeling strategy seems to be an expansion of the problem in powers of a small parameter $\epsilon \sim |\nabla h|/h \ll 1$, called the film parameter [11–13], since even in the strongly nonlinear regime the height h of the waves remains small when compared to their wavelength. In a second instance, at the moderate Reynolds numbers of interest, the flow is controlled by surface tension effects and viscous dissipation and, *via* the slaving principle [14], the latter is expected to permit the elimination of most local internal flow variables that are bound to follow the slow evolution of the film thickness (and possibly other local average flow quantities). The main idea underlying modeling attempts is

[a] e-mail: pops@ladhyx.polytechnique.fr

therefore to take advantage of this enslaving to reduce the space dimensionality of the problem by eliminating the cross-stream flow dependence and keeping explicit only the streamwise and possibly the spanwise space dependences.

The complete elimination of flow variables yields one-equation models governing the effective dynamics of the local film thickness. In the two-dimensional case, their general expression reads $\partial_t h = G(h^n, \partial_x{}^m h)$, where G involves various algebraic powers n and (streamwise) differentiation orders m of h. Their prototype is Benney's equation [11,12]:

$$\partial_t h + h^2 \partial_x h + \frac{1}{3}\partial_x \left[\left(\frac{2}{5} h^6 - B h^3 \right) \partial_x h + \Gamma h^3 \partial_{xxx} h \right] = 0 \tag{1}$$

that correctly describes the onset of the waves and their weakly nonlinear development analyzed within the framework of dynamical systems theory in [15]. In the limit of small amplitude modulations, equation (1) turns into a Kuramoto-Sivashinsky (KS) equation [16] thoroughly studied in [17,18].

Unfortunately, Benney's equation fails to reproduce the behavior of the film outside a close neighborhood of the threshold. Its solutions indeed experience finite-time blow-up at moderate Reynolds numbers, as shown in [15,19]. By contrast, neither the KS equation nor the full NS equations [6] or their BL approximation [8,20] seem to behave so wildly. The situation is not improved by pushing the gradient expansion to higher order, which leads to a more complicated equation [13] with no better properties. Though Ooshida has recently shown that this catastrophic behavior could be cured by regularizing the expansion using a Padé approximant technique [21], far from threshold, this remains insufficient and alternative approaches that do not lead to a single effective equation for the film thickness are needed.

Genuine modeling usually rests on low order truncations of weighted-residual approaches. In such methods, the primary aim of which is the search of specific solutions with given accuracy, the variables are expanded on a basis of test functions and one requires that the equations be fulfilled by projecting them on a series of weight functions and canceling the corresponding "residues".

A large spectrum of methods exist depending on the nature of the projection rule [22]. For example, in collocation methods weight functions are Dirac delta-functions centered at given points. The simplest integral method just asks that the equation be fulfilled on average. In the present problem, considering boundary-layer equations at lowest order and assuming that the velocity profile is parabolic, one obtains Shkadov's model [23]:

$$\partial_t h = -\partial_x q, \tag{2}$$

$$\partial_t q = h - 3\frac{q}{h^2} - \frac{12}{5}\frac{q}{h}\partial_x q + \left(\frac{6}{5}\frac{q^2}{h^2} - Bh \right) \partial_x h + \Gamma h \partial_{xxx} h, \tag{3}$$

which is apparently free of finite-time blow-up but fails to give a quantitatively accurate description of the instability threshold. The limitations of Shkadov's model derive from the lack of freedom in the description of the hydrodynamic fields and the too rustic character of the consistency condition expressed *via* the averaging. In order to improve over (3), Prokopiou *et al.* developed a second-order theory resting on the same simple averaging approach [24] at risk of finite-time singularities.

Refined approximations of the flow and/or other weighted residual methods have been developed in order to get better results. Improved models were obtained by expanding the hydrodynamic field on different functional bases of the cross-stream variable y, using various projection rules [25,26]. In some cases, center manifold techniques were exploited to eliminate strongly damped velocity modes, thus reducing the number of relevant governing fields [27]. In the absence of clear physical meaning for the coefficients appearing in the expansion, the interpretation of such studies was not straightforward and one was often confined to a comparison of the obtained output with that of concurrent models and numerical solutions of BL or NS equations, or with the results of laboratory experiments. A review of early modeling attempts can be found in [28].

In a previous paper [29], we derived one such model using a mixed integral-collocation method. It was written in terms of three partial differential equations for three coupled slowly varying fields, the thickness h of the film, the local flow rate q, and a supplementary variable τ measuring the departure of the wall shear stress from that predicted by a parabolic velocity profile. The velocity field was expanded on test functions that were the specific polynomials appearing in the derivation of Benney's equation. Though our model gave satisfactory results for the instability threshold and the shape of the waves at moderate distance from threshold, when compared to both laboratory experiments and direct numerical simulations (DNSs), it still suffered from finite-time blow-up sufficiently far from threshold.

In this paper we develop a systematic modeling strategy intended to overcome previously mentioned limitations and we show that the standard Galerkin method, in which the sets of test functions and weight functions are identical, yields the optimal model most economically. The convergence of various other approximations obtained by different weighted-residual methods towards this optimal model will be presented in a separate note [30]. The geometry of the problem and the set of primitive equations are recalled in Section 2. We demonstrate the expansion procedure in the two-dimensional case at first order in Section 3. The derivation of the second-order model is much more complicated. It is sketched in Section 4 where the final result is given, the complete calculation being developed elsewhere [31]. We then turn to the three-dimensional first-order model in Section 5 and extend it phenomenologically to second order. Finally, we compare different approximations and conclude in discussing prospective applications in Section 6.

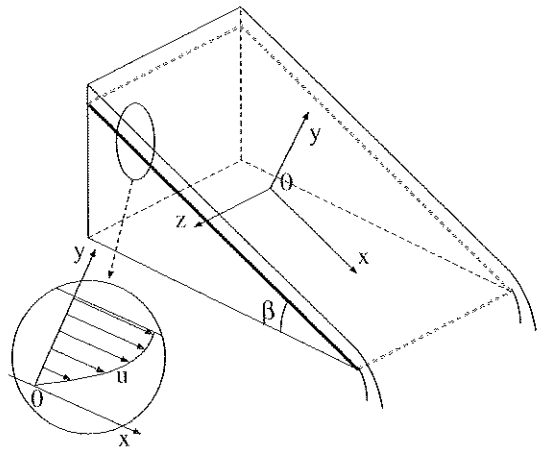

Fig. 1. Fluid film flowing down an inclined plane: definition of the geometry.

2 Governing equations

The geometry is defined in Figure 1. The inclined plane makes an angle β with the horizontal and $\hat{\mathbf{x}}$, $\hat{\mathbf{y}}$, and $\hat{\mathbf{z}}$ are unit vectors in the streamwise, cross-stream, and spanwise directions respectively. For the moment, we restrict ourselves to the two-dimensional case where the solution is independent of coordinate z. The supplementary terms arising in the three-dimensional case will be added in due course (Sect. 5).

Here we turn directly to dimensionless equations (see also [29]) and choose a scaling essentially defined from the fluid properties and the geometrical flow conditions avoiding any reference to the unperturbed film thickness or flow rate. The length and time units are constructed from g or rather $g\sin\beta$ (LT'^{-2}) and the kinematic viscosity $\nu = \mu/\rho$ ($L^2T'^{-1}$), which yields $L = \nu^{2/3}(g\sin\beta)^{-1/3}$ and $T' = \nu^{1/3}(g\sin\beta)^{-2/3}$ so that the velocity and pressure units read $U = LT'^{-1} = (\nu g\sin\beta)^{1/3}$ and $P = \rho(\nu g\sin\beta)^{2/3}$. The surface tension is then measured by the Kapitza number $\Gamma = \gamma/\left[\rho\nu^{4/3}(g\sin\beta)^{1/3}\right]$.

The basic 2D dimensionless equations read

$$\partial_t u + u\,\partial_x u + v\,\partial_y u = -\partial_x p + 1 + (\partial_{xx} + \partial_{yy})\,u, \quad (4)$$

$$\partial_t v + u\,\partial_x v + v\,\partial_y v = -\partial_y p - B + (\partial_{xx} + \partial_{yy})\,v, \quad (5)$$

$$\partial_x u + \partial_y v = 0 \quad (6)$$

where u and v are the streamwise (x) and cross-stream (y) velocity components, p is the pressure. Parameter $B = \cot\beta$, that measures the effects of the slope, is zero when the wall is vertical, $\beta = \pi/2$. These equations must be completed with boundary conditions at the free surface $y = h$ and the plate $y = 0$:

$$\partial_t h + u\big|_h\,\partial_x h = v\big|_h, \quad (7)$$

$$\frac{\Gamma\,\partial_{xx}h}{\left[1+(\partial_x h)^2\right]^{3/2}} + \frac{2}{1+(\partial_x h)^2}\left[\partial_x h\left(\partial_y u\big|_h + \partial_x v\big|_h\right) - (\partial_x h)^2\partial_x u\big|_h - \partial_y v\big|_h\right] + p\big|_h = 0, \quad (8)$$

$$2\partial_x h\left(\partial_y v\big|_h - \partial_x u\big|_h\right) + \left[1-(\partial_x h)^2\right]\left(\partial_y u\big|_h + \partial_x v\big|_h\right) = 0, \quad (9)$$

$$u\big|_0 = v\big|_0 = 0. \quad (10)$$

Equation (7) is the kinematic condition associated with the fact that the interface $h(x,t)$ is a material line, (8, 9) express the continuity of the normal and tangential components of the stress tensor at the interface and (10) stands for the no-slip condition at the rigid bottom.

Condition (7) at $y = h$ will be rewritten in integral form as

$$\partial_t h + \partial_x q = 0, \quad (11)$$

where $q(x,t) = \int_0^{h(x,t)} u(x,y,t)\mathrm{d}y$ is the local instantaneous flow rate. In this unit system where $g\sin\beta = \nu = \rho = 1$, the Reynolds number R is hidden in the boundary condition fixing the flat film Nusselt thickness h_N. The flow rate is indeed given by $q_\mathrm{N} = \frac{1}{3}h_\mathrm{N}^3$, which allows one to define the mean velocity u_N as $q_\mathrm{N}/h_\mathrm{N}$. Accordingly, $R = u_\mathrm{N}h_\mathrm{N}/\nu$ is numerically equal to q_N. Surface tension effects are often measured using the Weber number that reads $W = \Gamma/h_\mathrm{N}^2$.

3 Two-dimensional first-order model

The set of equations consistent at first order in the long-wavelength expansion ($\epsilon = |\partial_x h|/h \ll 1$), usually called the (first-order) boundary-layer equations by reference to the classical Prandtl's equations [32], then reads

$$\partial_t u + u\partial_x u + v\partial_y u - \partial_{yy}u = 1 - B\partial_x h + \Gamma\partial_{xxx}h, \quad (12)$$

$$\partial_x u + \partial_y v = 0, \quad (13)$$

$$\partial_y u\big|_h = 0, \quad (14)$$

$$u\big|_0 = v\big|_0 = 0, \quad (15)$$

along with (11) equation (12) is the only non-trivial component of the Navier-Stokes equations in the boundary layer approximation after elimination of the pressure. It should be noticed that the linear term $\Gamma\partial_{xxx}h$ on its right hand side is formally of third order and thus should not appear at this stage except when Γ is large enough so that it enters the problem at the same level as $\partial_x h$, *i.e.* $\Gamma\epsilon^2 = \mathcal{O}(1)$, which is the usual assumption made. Notice that the stress-free boundary condition (14) is homogeneous at this order. The incompressibility condition (13) also shows that the velocity component v is a slow variable. By contrast, the kinematic condition (11), which is in fact valid at all orders, relates slow variables to each other and will serve as a compatibility condition for the solution at every order.

Using the continuity equation (13) and the no-slip boundary condition (15) on v, one can replace v everywhere by $-\int_0^y \partial_x u\,\mathrm{d}y$ so that the only remaining dynamical variable is $u(x,y,t)$ which, according to the idea of

enslaving, is further searched by separation of variables as an expansion taken in the form

$$u(x,y,t) = \sum_j a_j(x,t) f_j(\bar{y}), \tag{16}$$

where $\bar{y}$ is the cross-stream coordinate rescaled by the local film thickness $h(x,t)$, *i.e.* $\bar{y} = y/h$. Both h and the expansion coefficients a_j are supposed to be slowly varying functions of time t and the streamwise coordinate x.

The fact that (i) the basic (Nusselt) flow profile is a semi-parabola, $u(y) \propto \bar{y}(1-\bar{y}/2)$, (ii) in Benney-like long wavelength expansions, corrections to this profile are polynomials in $\bar{y}$, (iii) the set of polynomials of increasing order forms a complete basis, (iv) this set is closed with respect to differentiations and products involved in the governing equations, makes it a reasonable choice to take polynomials as test functions.

A consistent first-order model can be obtained by considering a reduced set of test functions comprising monomials up to degree 6 included. This can be shown in the following way: assuming that the monomial of highest-degree retained in the expansion of u is $\bar{y}^n$, with coefficient c_n and n large enough (and > 2), let us differentiate (12) $n-2$ times with respect to y to get $\partial_{y^n} u = \partial_{y^{n-2}}(\partial_t u + u\partial_x u + v\partial_y u)$. The left hand side is then proportional to c_n, while the right hand side is obviously slowly varying. This implies that time-space derivatives of c_n are at least one order higher in the long-wavelength expansion. Repeating the argument while decreasing n, we immediately see that the same holds down to c_3 (cubic term). This is no longer the case for the coefficient c_2 of the quadratic term that must contain a zeroth-order contribution. Returning to (12) and considering inertial terms $\partial_t u + u\partial_x u + v\partial_y u$ we see that, since they involve supplementary differentiations with respect to the slow variables, or product with the slowly varying quantity v, in their evaluation we can neglect all terms involving the c_n with $n > 2$. We are thus left with a quadratic polynomial that generates monomials of fourth degree at most. In turn, the cancellation of these terms in the evolution equation can only be achieved by the terms arising from $\partial_{yy} u$, which will be possible if u is of degree 6, hence the result. Assuming that u is the most general degree-6 polynomial makes 7 unknown coefficients that can be reduced to 5 by taking boundary conditions (14, 15) into account. In fact, rather than the $\bar{y}^n$, it turns out convenient to expand u on the basis of test functions

$$f_j(\bar{y}) = \bar{y}^{j+1} - \tfrac{j+1}{j+2}\bar{y}^{j+2}, \tag{17}$$

that fulfills boundary conditions $f_j(0) = f_j'(1) = 0$ automatically. It is easily seen that the Nusselt solution is merely proportional to f_0. A first relation between the coefficients of the expansion and the thickness of the film is derived from (11) after explicit computation of $q = \int_0^h u\,\mathrm{d}y$:

$$\frac{3q}{h} = a_0 + \sum_{j=1}^{4} \frac{6}{(j+2)(j+3)} a_j. \tag{18}$$

Now, inserting the truncated expansion $u = \sum_{j=0}^{4} a_j f_j$ in equation (12) and neglecting all terms in a_j, $j > 0$ involving derivatives with respect to x and t we readily obtain a polynomial $\mathcal{P}(\bar{y})$ of degree 4 as inferred from the discussion above. Requiring the fulfillment of this equation by identifying all the coefficients of this polynomial, degree after degree, yields 5 equations for the 5 unknowns $a_j(x,t)$, $j = 0,\ldots,4$. We obtain:

$$0 = \frac{1}{h^2}(a_0 - 2a_1) - 1 + B\partial_x h - \Gamma\partial_{xxx} h, \tag{19}$$

$$0 = \frac{1}{h^2}(4a_1 - 6a_2) + \partial_t a_0 - \frac{a_0}{h}\partial_t h, \tag{20}$$

$$0 = \frac{1}{h^2}(9a_2 - 12a_3) - \frac{1}{2}\partial_t a_0 + \frac{a_0}{h}\partial_t h + \frac{1}{2}a_0\partial_x a_0 - \frac{a_0^2}{2h}\partial_x h, \tag{21}$$

$$0 = \frac{1}{h^2}(16a_3 - 20a_4) - \frac{1}{3}a_0\partial_x a_0 + \frac{2a_0^2}{3h}\partial_x h, \tag{22}$$

$$0 = \frac{1}{h^2}25a_4 + \frac{1}{6}\left(\frac{1}{2}a_0\partial_x a_0 - \frac{a_0^2}{h}\partial_x h\right). \tag{23}$$

Equations (20–23) determine the four unknowns $a_1,\ldots,a_4$ in terms of a_0 and h and their space-time derivatives. They can thus be eliminated by inserting their expressions into (19), which leads to

$$a_0 = h^2 - \frac{1}{3}h^2\partial_t a_0 + \frac{1}{6}ha_0\partial_t h - \frac{1}{10}h^2 a_0\partial_x a_0 + \frac{1}{30}ha_0^2\partial_x h - Bh^2\partial_x h + \Gamma h^2\partial_{xxx} h. \tag{24}$$

In the same way, (18) reads:

$$q = \frac{1}{3}ha_0 - \frac{1}{45}h^3\partial_t a_0 + \frac{1}{360}h^2 a_0\partial_t h - \frac{3}{280}h^3 a_0\partial_x a_0 + \frac{1}{504}h^2 a_0^2\partial_x h. \tag{25}$$

The system formed by (24, 11) with q given by (25) is then closed for h and a_0. However a_0 is not an intrinsic variable since it depends on the choice of the test functions and it turns out preferable to express the model in terms of the flow rate q which is intrinsic. Combining (25) and (24) we get

$$0 = \frac{3q}{h} - h^2 + \frac{2}{5}h^2\partial_t a_0 - \frac{7}{40}ha_0\partial_t h + \frac{37}{280}h^2 a_0\partial_x a_0 + \frac{11}{280}ha_0^2\partial_x h + Bh^2\partial_x h - \Gamma h^2\partial_{xxx} h.$$

At first order in the long-wavelength expansion we can replace a_0 by $3q/h$ in this equation and further use the identity $\partial_t h = -\partial_x q$ to obtain

$$\partial_t q = \frac{5}{6}h - \frac{5}{2}\frac{q}{h^2} - \frac{17}{7}\frac{q}{h}\partial_x q + \left(\frac{9}{7}\frac{q^2}{h^2} - \frac{5}{6}Bh\right)\partial_x h + \frac{5}{6}\Gamma h\partial_{xxx} h, \tag{26}$$

which, together with (11), constitutes a consistent first-order model.

System (11, 26) can be taken as a primitive problem on which to perform a long-wavelength expansion. We assume $q = q^{(0)} + q^{(1)}$ where the superscript denotes the order in differentiation ∂_x and $\Gamma\epsilon^2 = \mathcal{O}(1)$. At zeroth order it yields: $0 = \frac{5}{6}h - \frac{5}{2}q^{(0)}/h^2$, therefore $q^{(0)} = \frac{1}{3}h^3$ as expected. At first order we get

$$\partial_t q^{(0)} = -\frac{5}{2}\frac{q^{(1)}}{h^2} - \frac{17}{7}\frac{q^{(0)}}{h}\partial_x q^{(0)} + \left(\frac{9}{7}\left(\frac{q^{(0)}}{h}\right)^2 - \frac{5}{6}Bh\right)\partial_x h + \frac{5}{6}\Gamma h\partial_{xxx}h.$$

Making use of the expression of $q^{(0)}$ and substituting $-\partial_x q^{(0)}$ to $\partial_t h$ we obtain $q^{(1)} = \left(\frac{2}{15}h^6 - \frac{1}{3}Bh^3\right)\partial_x h + \frac{1}{3}\Gamma h^3\partial_{xxx}h$ which in turn leads back to Benney's equation (1) when inserted in $\partial_t h + \partial_x\left(q^{(0)} + q^{(1)}\right) = 0$.

Equation (26) can be obtained in a simpler way by means of a standard Galerkin method. This results from a specific feature of the method that uses for weight functions the test functions themselves which, in turn, are supposed to fulfill the boundary conditions. When applied to (12), in the general case the projection step reads

$$\int_0^h f_j(y/h)(\partial_t u + u\partial_x u + v\partial_y u - \partial_{yy}u)\mathrm{d}y = \frac{2h}{(j+2)(j+3)}(1 - B\partial_x h + \Gamma\partial_{xxx}h), \quad (27)$$

of which only the term $\int_0^h f_j(y/h)\partial_{yy}u\,\mathrm{d}y$ is of special concern. Through a double integration by parts using boundary conditions $f_j(0) = 0$ and $f_j'(1) = 0$, in full generality this term reads $\int_0^h u f_j''(\bar{y})\,\mathrm{d}y$. In the case $j = 0$ for which $f_0''(\bar{y}) \equiv -1$ we get

$$\int_0^h f_0(y/h)\partial_{yy}u\,\mathrm{d}y = -\frac{q}{h^2} \quad (28)$$

by definition of $q = \int_0^h u\,\mathrm{d}y$, *i.e.* the very special combination of the a_i given by (18) we need to close the model. For $j > 0$, we get a linear system that can be solved for the a_j, $j > 0$ as a function of a_0, hence bringing no constraint on the evolution, while being of use to reconstruct the flow pattern. Since a_0 and $3q/h$ are interchangeable in all terms containing derivatives in x or t when computing (27) for $j = 0$ at the considered order, equation (26) follows immediately from this evaluation, namely

$$\frac{2}{15}h\partial_t a_0 - \frac{7}{120}a_0\partial_t h + \frac{37}{840}ha_0\partial_x a_0 - \frac{11}{840}a_0^2\partial_x h + \frac{q}{h^2} = \frac{1}{3}(h - Bh\partial_x h + \Gamma h\partial_{xxx}h)$$

when making use of (11). A similar property of the Galerkin method will be shown below to simplify also the second-order computation.

4 Two-dimensional second-order model

Now having fully developed our strategy at first-order, let us sketch the main steps leading to a model consistent at second-order. Equation (12) and boundary condition (14) have to be completed. They read [29]

$$\partial_t u + u\partial_x u + v\partial_y u - \partial_{yy}u - 2\partial_{xx}u = 1 + \partial_x\left[\partial_x u|_h\right] - B\partial_x h + \Gamma\partial_{xxx}h, \quad (29)$$

$$\partial_y u|_h = 4\partial_x h\partial_x u|_h - \partial_x v|_h. \quad (30)$$

Transposing the argument leading to the conclusion that the first order approximation to u is a polynomial of degree 6 now implies that the second order approximation is a polynomial of degree 14 (inertial term is formally quadratic, hence of degree 12, and has to be compensated by a term originating from $\partial_{yy}u$, hence u of degree 14). The general solution thus depends on h plus 14 supplementary coefficients (condition $u|_0 = 0$ suppresses one coefficient) and though their determination by identification is still possible, it seems reasonable to find a short-cut, which will be achieved in three steps: (i) determine the number of independent fields required to insure consistency at second order (in addition to h, only one, namely q, was necessary at first order); (ii) construct a basis of test functions that takes (i) into account (the fact that $\partial_y u$ no longer cancels at $y = h$ makes the f_j less appropriate); (iii) show that the projection of the evolution equations onto this reduced set of test functions yields the result most economically.

(i) The solution for u is given by expansion (16) with coefficients derived from (20–23). In fact, when the first order equivalence $a_0 = 3q/h$ and the mass conservation condition $\partial_t h = -\partial_x q$ have been used, the a_j are not independent and one can verify that

$$a_1 + 3a_2 = -4a_3 = 20a_4 = -\frac{3}{5}h^3 q\partial_x(q/h^3). \quad (31)$$

The velocity field at first order can thus be written as

$$u = 3\frac{q}{h}f_0 + a_1\left(-\frac{2}{5}f_0 + f_1 - \frac{1}{3}f_2\right) + a_3\left(\frac{8}{35}f_0 - \frac{4}{3}f_2 + f_3 - \frac{1}{5}f_4\right), \quad (32)$$

hence as a combination of three independent fields (q/h, a_1, a_3) rather than five as could be expected naively. The new fields a_1 and a_3 contribute to the second order through the inertial term on the left-hand side of (29). Three independent conditions will thus be required to determine their evolution consistently.

(ii) In order to take advantage of the specific form of u given by (32), it is advisable to let aside the f_j, $j > 0$, and to turn to appropriate combinations of the test functions that appear in this expression. Let us denote them as g_j for clarity. Keeping $g_0 \equiv f_0$, we choose g_1 as a combination of f_0 and $f_1 - \frac{1}{3}f_2$, and g_2 as a combination of f_0, $f_1 - \frac{1}{3}f_2$,

and $-\frac{4}{3}f_2 + f_3 - \frac{1}{5}f_4$. Proceeding for later convenience to a Schmidt orthogonalization — so that the correspondent flow components present themselves as corrections to the basic profile in a least-square sense — we arrive at

$$g_0 = \bar{y} - \tfrac{1}{2}\bar{y}^2, \tag{33}$$

$$g_1 = \bar{y} - \tfrac{17}{6}\bar{y}^2 + \tfrac{7}{3}\bar{y}^3 - \tfrac{7}{12}\bar{y}^4, \tag{34}$$

$$g_2 = \bar{y} - \tfrac{13}{2}\bar{y}^2 + \tfrac{57}{4}\bar{y}^3 - \tfrac{111}{8}\bar{y}^4 + \tfrac{99}{16}\bar{y}^5 - \tfrac{33}{32}\bar{y}^6. \tag{35}$$

The basis is then completed by other independent polynomials of increasing degree, the expressions of which have no importance since, as shown below, the Galerkin procedure avoids the determination of their coefficients. Note however that, because the boundary condition at the interface (30) is no longer independent of coordinate x, it cannot be included in the definition of the test functions but has to be added to the set of constraints [33].

(iii) We have now to evaluate the residues

$$\int_0^h g_j(y/h)(\partial_t u + u\partial_x u + v\partial_y u - \partial_{yy}u - 2\partial_{xx}u)\mathrm{d}y$$
$$= h\left(1 + \partial_x\left[\partial_x u|_h\right] - B\partial_x h + \Gamma\partial_{xxx}h\right])\int_0^h g_j\,\mathrm{d}y. \tag{36}$$

It is readily seen that the first order evaluation of u is sufficient for the computation of the inertial term, the term $-2\partial_{xx}u$, and the term $\partial_x[\partial_x u|_h]$ on the right hand side of (36) since they all involve additional slow space-time derivatives. So, the problem is to show that, for $j = 0, 1, 2$, the remaining linear terms can be computed in closed form, *i.e.* without introducing coefficients of the g_j with $j \neq 0, 1, 2$. This is indeed the case since by performing two successive integrations by parts we get:

$$\int_0^h g_j(\bar{y})\partial_{yy}u\,\mathrm{d}y = \left[g_j\partial_y u\right]_0^h - \frac{1}{h}\left[g_j' u\right]_0^h + \frac{1}{h^2}\int_0^h g_j'' u\,\mathrm{d}y.$$

where primes denote $\bar{y}$-differentiation. The right-hand side of this equation can be simplified by using boundary conditions (15, 30) and the fact that the g_j, $j = 0, 1, 2$, are linear combinations of the f_j, $j = 0, \ldots, 4$, that fulfill $f_j'(1) = 0$. The integrated terms are then reduced to a single one, namely $g_j(1)[4\partial_x h\partial_x u|_h - \partial_x v|_h]$, that can be evaluated explicitly within the ansatz at the requested order. The argument about the closure is concluded by noticing that $g_0'' \equiv -1$, $g_1'' \equiv 14g_0 - \frac{17}{3}$, and $g_2'' = \frac{1485}{28}g_1 + \frac{909}{28}g_0 - 13$, thus introducing no other functions of $\bar{y}$ than those of the considered reduced set.

A consistent second-order model is therefore obtained by inserting $u = b_0(x,t)g_0(\bar{y}) + b_1(x,t)g_1(\bar{y}) + b_2(x,t)g_2(\bar{y})$ into (36) with $j = 0, 1, 2$, and adding the continuity equation (11) with q given by $\int_0^h u\,\mathrm{d}y$. In practice, it turns out convenient to define

$$b_0 \equiv 3\frac{q - s_1 - s_2}{h}, \quad b_1 \equiv 45\frac{s_1(x,t)}{h},$$
$$b_2 \equiv 210\frac{s_2(x,t)}{h}, \tag{37}$$

in order to implement the condition $\int_0^h u\,\mathrm{d}y = q$ from the start. This choice has the virtue of making the corrections s_1 and s_2 homogeneous to q thus leading to equations with a similar structure. A tedious computation requiring the assistance of formal algebra [31] leads to

$$\begin{aligned}\partial_t q = {} & \frac{27}{28}h - \frac{81}{28}\frac{q}{h^2} - 33\frac{s_1}{h^2} - \frac{3069}{28}\frac{s_2}{h^2} - \frac{12}{5}\frac{qs_1\partial_x h}{h^2} \\ & - \frac{126}{65}\frac{qs_2\partial_x h}{h^2} + \frac{12}{5}\frac{s_1\partial_x q}{h} + \frac{171}{65}\frac{s_2\partial_x q}{h} + \frac{12}{5}\frac{q\partial_x s_1}{h} \\ & + \frac{1017}{455}\frac{q\partial_x s_2}{h} + \frac{6}{5}\frac{q^2\partial_x h}{h^2} - \frac{12}{5}\frac{q\partial_x q}{h} + \frac{5025}{896}\frac{q(\partial_x h)^2}{h^2} \\ & - \frac{5055}{896}\frac{\partial_x q\partial_x h}{h} - \frac{10851}{1792}\frac{q\partial_{xx}h}{h} + \frac{2027}{448}\partial_{xx}q \\ & - \frac{27}{28}Bh\,\partial_x h + \frac{27}{28}\Gamma h\partial_{xxx}h, \end{aligned} \tag{38}$$

$$\begin{aligned}\partial_t s_1 = {} & \frac{1}{10}h - \frac{3}{10}\frac{q}{h^2} - \frac{3}{35}\frac{q^2\partial_x h}{h^2} - \frac{126}{5}\frac{s_1}{h^2} - \frac{126}{5}\frac{s_2}{h^2} \\ & + \frac{1}{35}\frac{q\partial_x q}{h} + \frac{108}{55}\frac{qs_1\partial_x h}{h^2} - \frac{5022}{5005}\frac{qs_2\partial_x h}{h^2} \\ & - \frac{103}{55}\frac{s_1\partial_x q}{h} + \frac{9657}{5005}\frac{s_2\partial_x q}{h} - \frac{39}{55}\frac{q\partial_x s_1}{h} \\ & + \frac{10557}{10010}\frac{q\partial_x s_2}{h} + \frac{93}{40}\frac{q\left(\partial_x h\right)^2}{h^2} - \frac{69}{40}\frac{\partial_x h\partial_x q}{h} \\ & + \frac{21}{80}\frac{q\partial_{xx}h}{h} - \frac{9}{40}\partial_{xx}q - \frac{1}{10}Bh\partial_x h \\ & + \frac{1}{10}\Gamma h\partial_{xxx}h, \end{aligned} \tag{39}$$

$$\begin{aligned}\partial_t s_2 = {} & \frac{13}{420}h - \frac{13}{140}\frac{q}{h^2} - \frac{39}{5}\frac{s_1}{h^2} - \frac{11817}{140}\frac{s_2}{h^2} - \frac{4}{11}\frac{qs_1\partial_x h}{h^2} \\ & + \frac{18}{11}\frac{qs_2\partial_x h}{h^2} - \frac{2}{33}\frac{s_1\partial_x q}{h} - \frac{19}{11}\frac{s_2\partial_x q}{h} + \frac{6}{55}\frac{q\partial_x s_1}{h} \\ & - \frac{288}{385}\frac{q\partial_x s_2}{h} - \frac{3211}{4480}\frac{q\left(\partial_x h\right)^2}{h^2} + \frac{2613}{4480}\frac{\partial_x h\partial_x q}{h} \\ & - \frac{2847}{8960}\frac{q\partial_{xx}h}{h} + \frac{559}{2240}\partial_{xx}q - \frac{13}{420}Bh\partial_x h \\ & + \frac{13}{420}\Gamma h\partial_{xxx}h. \end{aligned} \tag{40}$$

Note that, by performing a gradient expansion with the assumptions $q = q^{(0)} + q^{(1)} + q^{(2)}$, $s_{1,2} = s_{1,2}^{(1)} + s_{1,2}^{(2)}$, one recovers the exact asymptotic result at second order [13].

The complete expression of the second order model is therefore somewhat involved. A much simpler model is obtained by assuming s_1 and s_2 to be of higher order than second order. Thus, their derivatives or products with h or q-derivatives can be dropped so that they only enter into the calculation *via* the terms $\frac{1}{h^2}\int_0^h g_j'' u\,\mathrm{d}y$ appearing in the evaluation of the residues (36) as noticed previously. Within this crude assumption and because $g_0'' = -1$, s_1 and s_2 do not appear into the evaluation of the first residue. Thus applying the Galerkin method to the second-order problem (36) but with a single function g_0 leads to

the consistency condition:

$$\partial_t q = \frac{5}{6}h - \frac{5}{2}\frac{q}{h^2} - \frac{17}{7}\frac{q}{h}\partial_x q + \left(\frac{9}{7}\frac{q^2}{h^2} - \frac{5}{6}Bh\right)\partial_x h + 4\frac{q}{h^2}(\partial_x h)^2 - \frac{9}{2h}\partial_x q\partial_x h - 6\frac{q}{h}\partial_{xx}h + \frac{9}{2}\partial_{xx}q + \frac{5}{6}\Gamma h\partial_{xxx}h. \quad (41)$$

The new terms are on the second line. They are all generated by the second-order contributions coming from $2\partial_{xx}u + \partial_x[\partial_x u|_h]$ in the momentum equation (29) and the boundary condition (30). As such they include the effect of viscous dispersion that was lacking at first order. Hereafter equations (11, 41) will be referred to as the second-order simplified Galerkin model.

The expansion of (11, 41) now yields

$$\begin{aligned} q^{(0)} &= \frac{1}{3}h^3, \\ q^{(1)} &= \left(\frac{2}{15}h^6 - \frac{1}{3}Bh^3\right)\partial_x h + \frac{\Gamma}{3}h^3\partial_{xxx}h, \\ q^{(2)} &= \left(\frac{7}{3}h^3 - \frac{8}{15}Bh^6 + \frac{212}{525}h^9\right)(\partial_x h)^2 \\ &\quad + \left(h^4 - \frac{10}{63}Bh^7 + \frac{4}{63}h^{10}\right)\partial_{xx}h \\ &\quad + \Gamma h^5\left(\frac{8}{5}(\partial_x h)^2\partial_{xx}h + \frac{4}{5}h(\partial_{xx}h)^2 \right. \\ &\quad \left. + \frac{4}{3}h\partial_x h\partial_{xxx}h + \frac{10}{63}h^2\partial_{x^4}h\right), \end{aligned}$$

and, remarkably enough, only the coefficient of the term $h^9(\partial_x h)^2$ in the expression of $q^{(2)}$ differs from the exact result $\frac{127}{315}$, by a relative factor as small as 0.2%. Indeed, the monomials of highest degrees appearing in the gradient expansion contribute very little to the result (see the discussion in [29]). Equation (41) is thus the result of the application of Galerkin method using g_0 only and therefore does not take into account the corrections to the parabolic profile introduced by s_1 and s_2.

Before comparing the performances of the different models in Section 6, let us now turn to their three-dimensional extension.

5 Three-dimensional models

At order zero in the long-wavelength expansion, the flow is uniform and purely streamwise. A spanwise component $w \neq 0$ appears as soon as it ceases to be two-dimensional (in x and y) as a result of the deformation of the interface in the z-direction. It is therefore a slowly varying quantity, the space or time derivatives of which can then be dropped at first order. The spanwise component of the Navier-Stokes equations that simply reads

$$\partial_{yy}w = B\partial_z h - \Gamma(\partial_{xxz} + \partial_{zzz})h, \quad (42)$$

has thus to be added to the original system in which equation (12) must be completed to account for the spanwise dependence:

$$\partial_t u + u\partial_x u + v\partial_y u - \partial_{yy}u = 1 - B\partial_x h + \Gamma(\partial_{xxx} + \partial_{xzz})h. \quad (43)$$

The velocity component w is submitted to the boundary conditions

$$w|_0 = 0, \quad \partial_y w|_h = 0. \quad (44)$$

Equation (42) is readily integrated to yield

$$w = -[B\partial_z h - \Gamma(\partial_{xxz} + \partial_{zzz})h]f_0(y/h), \quad (45)$$

where $f_0(\bar{y}) = \bar{y} - \frac{1}{2}\bar{y}^2$ as before. At this order, the spanwise flow component is therefore fully slaved to the thickness h of the film. Denoting the streamwise flow rate q by $q_\parallel$ and defining the spanwise flow rate as $q_\perp = \int_0^h w\,\mathrm{d}y$, we can write the kinematic boundary condition at the interface $v|_h = \partial_t h + u|_h\partial_x h + w|_h\partial_z h$ in flux form as

$$\partial_t h + \partial_x q_\parallel + \partial_z q_\perp = 0, \quad (46)$$

in which the last term is known once h is determined:

$$q_\perp = -\tfrac{1}{3}h^3\left(B\partial_z h - \Gamma(\partial_{xxz} + \partial_{zzz})h\right). \quad (47)$$

The same procedure as in the two-dimensional case then yields:

$$\partial_t q_\parallel = \frac{5}{6}h - \frac{5}{2}\frac{q_\parallel}{h^2} - \frac{17}{7}\frac{q_\parallel}{h}\partial_x q_\parallel + \left(\frac{9}{7}\frac{q_\parallel^2}{h^2} - \frac{5}{6}Bh\right)\partial_x h + \frac{5}{6}\Gamma h(\partial_{xxx} + \partial_{xzz})h. \quad (48)$$

The three-dimensional first-order model is therefore given by (48, 46) where $q_\perp$ is given by (47).

At second-order the derivatives of $q_\perp$ cannot be neglected so that $q_\perp$ is an effective degree of freedom on its own. Following the same method as for the two-dimensional case, let us write w as

$$w = 3\frac{q_\perp}{h}f_0(\bar{y}). \quad (49)$$

Therefore using (49, 37), where s_1 and s_2 are now functions of z, the Galerkin method leads to

$$\begin{aligned} \partial_t q_\parallel &= \frac{27}{28}h - \frac{81}{28}\frac{q_\parallel}{h^2} - 33\frac{s_1}{h^2} - \frac{3069}{28}\frac{s_2}{h^2} - \frac{12}{5}\frac{q_\parallel s_1\partial_x h}{h^2} \\ &\quad - \frac{126}{65}\frac{q_\parallel s_2\partial_x h}{h^2} + \frac{12}{5}\frac{s_1\partial_x q_\parallel}{h} + \frac{171}{65}\frac{s_2\partial_x q_\parallel}{h} + \frac{12}{5}\frac{q_\parallel\partial_x s_1}{h} \\ &\quad + \frac{1017}{455}\frac{q_\parallel\partial_x s_2}{h} + \frac{6}{5}\frac{q_\parallel^2\partial_x h}{h^2} - \frac{12}{5}\frac{q_\parallel\partial_x q_\parallel}{h} \\ &\quad + \frac{5025}{896}\frac{q_\parallel(\partial_x h)^2}{h^2} - \frac{5055}{896}\frac{\partial_x q_\parallel\partial_x h}{h} - \frac{10851}{1792}\frac{q_\parallel\partial_{xx}h}{h} \\ &\quad + \frac{2027}{448}\partial_{xx}q_\parallel - \frac{27}{28}Bh\,\partial_x h + \frac{27}{28}\Gamma h\,(\partial_{xxx} + \partial_{xzz})\,h \\ &\quad - \frac{6}{5}\frac{q_\parallel\partial_z q_\perp}{h} - \frac{6}{5}\frac{q_\perp\partial_z q_\parallel}{h} + \frac{6}{5}\frac{q_\parallel q_\perp\partial_z h}{h^2} - \frac{2463}{1792}\frac{\partial_z q_\parallel\partial_z h}{h} \\ &\quad + \frac{2433}{1792}\frac{q_\parallel(\partial_z h)^2}{h^2} - \frac{5361}{3584}\frac{q_\parallel\partial_{zz}h}{h} + \partial_{zz}q_\parallel\,, \end{aligned} \quad (50)$$

$$\partial_t s_1 = \frac{1}{10}h - \frac{3}{10}\frac{q_\parallel}{h^2} - \frac{3}{35}\frac{q_\parallel^2\partial_x h}{h^2} - \frac{126}{5}\frac{s_1}{h^2} - \frac{126}{5}\frac{s_2}{h^2} + \frac{1}{35}\frac{q_\parallel\partial_x q_\parallel}{h} + \frac{108}{55}\frac{q_\parallel s_1\partial_x h}{h^2} - \frac{5022}{5005}\frac{q_\parallel s_2\partial_x h}{h^2} - \frac{103}{55}\frac{s_1\partial_x q_\parallel}{h} + \frac{9657}{5005}\frac{s_2\partial_x q_\parallel}{h} - \frac{39}{55}\frac{q_\parallel\partial_x s_1}{h} + \frac{10557}{10010}\frac{q_\parallel\partial_x s_2}{h} + \frac{93}{40}\frac{q_\parallel(\partial_x h)^2}{h^2} - \frac{69}{40}\frac{\partial_x h\partial_x q_\parallel}{h} + \frac{21}{80}\frac{q_\parallel\partial_{xx}h}{h} - \frac{9}{40}\partial_{xx}q_\parallel - \frac{1}{10}Bh\partial_x h + \frac{1}{10}\Gamma h\left(\partial_{xxx}+\partial_{xzz}\right)h - \frac{2}{35}\frac{q_\parallel\partial_z q_\perp}{h} + \frac{3}{35}\frac{q_\perp\partial_z q_\parallel}{h} - \frac{3}{35}\frac{q_\parallel q_\perp\partial_z h}{h^2} - \frac{57}{80}\frac{\partial_z q_\parallel\partial_z h}{h} + \frac{81}{80}\frac{q_\parallel(\partial_z h)^2}{h^2} - \frac{3}{40}\frac{q_\parallel\partial_{zz}h}{h}, \tag{51}$$

$$\partial_t s_2 = \frac{13}{420}h - \frac{13}{140}\frac{q_\parallel}{h^2} - \frac{39}{5}\frac{s_1}{h^2} - \frac{11817}{140}\frac{s_2}{h^2} - \frac{4}{11}\frac{q_\parallel s_1\partial_x h}{h^2} + \frac{18}{11}\frac{q_\parallel s_2\partial_x h}{h^2} - \frac{2}{33}\frac{s_1\partial_x q_\parallel}{h} - \frac{19}{11}\frac{s_2\partial_x q_\parallel}{h} + \frac{6}{55}\frac{q_\parallel\partial_x s_1}{h} - \frac{288}{385}\frac{q_\parallel\partial_x s_2}{h} - \frac{3211}{4480}\frac{q_\parallel(\partial_x h)^2}{h^2} + \frac{2613}{4480}\frac{\partial_x h\partial_x q_\parallel}{h} - \frac{2847}{8960}\frac{q_\parallel\partial_{xx}h}{h} + \frac{559}{2240}\partial_{xx}q_\parallel - \frac{13}{420}Bh\partial_x h + \frac{13}{420}\Gamma h\left(\partial_{xxx}+\partial_{xzz}\right)h + \frac{3029}{8960}\frac{\partial_z q_\parallel\partial_z h}{h} - \frac{3627}{8960}\frac{q_\parallel(\partial_z h)^2}{h^2} + \frac{299}{17920}\frac{q_\parallel\partial_{zz}h}{h}, \tag{52}$$

$$\partial_t q_\perp = -\frac{5}{2}\frac{q_\perp}{h^2} + \frac{9}{7}\frac{q_\parallel q_\perp\partial_x h}{h^2} - \frac{8}{7}\frac{q_\perp\partial_x q_\parallel}{h} - \frac{9}{7}\frac{q_\parallel\partial_x q_\perp}{h} + \frac{13}{4}\frac{q_\parallel\partial_x h\partial_z h}{h^2} - \frac{43}{16}\frac{\partial_z q_\parallel\partial_x h}{h} - \frac{13}{16}\frac{\partial_x q_\parallel\partial_z h}{h} - \frac{73}{16}\frac{q_\parallel\partial_{xz}h}{h} + \frac{7}{2}\partial_{xz}q_\parallel - \frac{5}{6}Bh\,\partial_z h + \frac{5}{6}\Gamma h\left(\partial_{xxz}+\partial_{zzz}\right)h, \tag{53}$$

to which the mass conservation law (46) needs to be added. Again, the full second-order model appears to be very complicated, which severely limits its use. Nevertheless, a simpler, though approximate, model can again be derived from the Galerkin method applied to the parabolic profile. The corresponding simplified three-dimensional model is then made of

$$\partial_t q_\parallel = \frac{5}{6}h - \frac{5}{2}\frac{q_\parallel}{h^2} + \frac{9}{7}\frac{q_\parallel^2\partial_x h}{h^2} - \frac{17}{7}\frac{q_\parallel\partial_x q_\parallel}{h} - \frac{97}{56}\frac{q_\parallel\partial_z q_\perp}{h} - \frac{9}{7}\frac{q_\perp\partial_z q_\parallel}{h} + \frac{129}{56}\frac{q_\parallel q_\perp\partial_z h}{h^2} + 4\frac{q(\partial_x h)^2}{h^2} - \frac{9}{2}\frac{\partial_x q_\parallel\partial_x h}{h} - 6\frac{q_\parallel\partial_{xx}h}{h} - \frac{\partial_z q_\parallel\partial_z h}{h} + \frac{3}{4}\frac{q_\parallel(\partial_z h)^2}{h^2} - \frac{23}{16}\frac{q_\parallel\partial_{zz}h}{h} + \frac{9}{2}\partial_{xx}q_\parallel + \partial_{zz}q_\parallel - \frac{5}{6}Bh\,\partial_x h + \frac{5}{6}\Gamma h\left(\partial_{xxx}+\partial_{xzz}\right)h, \tag{54}$$

together with (53, 46).

6 Discussion

In this paper, we have developed a systematic strategy to derive, from the primitive equations, systems with reduced physical dimensionality that we call models. The derivation is based on an expansion at first or second order in the streamwise gradient in order to recover asymptotic results close to the instability threshold. Weighted-residual techniques with polynomial test functions are used to eliminate the cross-stream dependence thought to be irrelevant. A conventional Galerkin method has been shown to yield the sought result most economically and consistency at a given order can be obtained through the evaluation of a small number of residuals, only one instead of five at first order, and three instead of fourteen at second order. The second-order model turns out to have a very complicated structure that limits its usefulness, whereas the first-order model is much simpler but ignores some important physical effects such as the dispersion introduced by viscosity. Applying the Galerkin method with a set of test functions reduced to the semi-parabolic basic flow profile leads to a simplified but approximate second-order model taking into account some dominant physical effects while remaining sufficiently tractable, especially concerning its three-dimensional extension.

At this stage, it should be stressed that the first-order model (11, 26), as well as the full second order model (11, 38–40), each at its level, are optimal in the sense that any weighted residual method based on polynomial functions (both test and weight functions) can be shown to converge to them. The convergence properties of several methods will be analyzed elsewhere [30]. Let us just mention that, unfortunately, the integral-collocation method we used in [29] has in fact bad convergence properties. By contrast, instead of placing a collocation condition at the plate, *i.e.* far from the surface where the instability mechanism is at work [34], the Galerkin method performs a weighted average that turns out to be most effective in the present case. However, this does not guarantee us yet that some progress has been achieved concerning the validity of our models deep inside the nonlinear domain. So, in the following we examine them from the point of view of the existence and properties of the strongly nonlinear

two-dimensional waves they generate beyond threshold, and compare our results with those published previously in the relevant literature which we are aware of. The study of the three-dimensional properties and secondary instabilities against transverse modes is in progress and will be the subject of another publication [35].

Two-dimensional waves that propagate without deformation at speed c along the inclined plane are special solutions of a dynamical system written in terms of a variable $\xi = x - ct$ and obtained in the standard way from the set of partial differential equations in x and t. Solitary waves correspond to homoclinic solutions joining some fixed point to itself, along the intersection of the unstable manifold and the stable manifold that nonlinearly extrapolate the linear subspaces accounting for the stability properties of this fixed point. Periodic wave-trains are described in the same way by limit cycles in the system's phase space.

The continuation software AUTO97 and the homoclinic bifurcation package HOMCONT [36] have been used to obtain periodic wave-trains and one-hump solitary wave solutions, with a special attention to the determination of the speed and the shape of the waves. Concerning models others than ours, most of the time no meaningful quantitative comparisons could be drawn from the original publications. This situation obliged us to perform our own computations using the same methodology but applied to the corresponding analytical formulations found in the literature. Previous results, when available, are closely recovered, *e.g.* those in [21,28,37] after proper implementation of notational changes. In order to stick to the common use and characterize the flow conditions, we now pass from the Nusselt thickness $h_{\rm N}$ to the Reynolds number $R = \frac{1}{3}h_{\rm N}^3$ and, occasionally, from the Kapitza number Γ to the Weber number $W = \Gamma/h_{\rm N}^2$.

Figures 2 and 3 display our results for the speed of one-hump solitary waves (left) and their maximum height (right) as functions of the Reynolds number in the case of a vertical plane and for various models. The physical parameters correspond to the mixture of glycerol and water used in experiments performed by Gollub *et al.* [5], *i.e.* $\Gamma = 252$. Here the speed c is rescaled by $3u_{\rm N}$ where $u_{\rm N}$ is the average velocity of the flat film solution, so that the phase speed of linear waves at criticality is equal to one. In the same way, the height of the waves is rescaled by the Nusselt thickness $h_{\rm N}$. Figure 3 is a close-up at low Reynolds numbers that illustrates the grouping of the curves according to the order of approximation in the long wavelength expansion. We are not aware of DNSs of the Navier-Stokes equations corresponding to the chosen conditions. This suggested us to take for reference the results that we believe to be the most reliable, *i.e.* those obtained with our full two-dimensional second-order model (Curves 7) in order to discuss the various models considered.

Let us begin with models in terms of a single "surface equation" (for the film thickness h). Curves 0 accounts for the results obtained with Benney's equation (1) which is asymptotically valid close to onset of waves occurring at zero Reynolds number. As already known [15], this curve turns back at $R \approx 1.49$ beyond which no one-hump solitary wave can be found. The upper part of the curve corresponds to unstable waves and, right at the saddle-node bifurcation, the maximum height of the wave is about 1.4 only, which clearly indicates that the applicability of the equation is restricted to very small amplitudes. The second-order Benney's equation, equation (11) in [13], yields Curves 1, from which we see that the additional terms do not improve the situation since the turnback takes place at an even lower Reynolds number. This illustrates the lack of convergence of the expansion method motivating Ooshida's regularization attempt by an adaptation of the Padé approximant method [21]. The success of this attempt is confirmed by Curves 2, from which one understands that the main deficiency of the primitive series of surface equations has been cured: one-hump solitary waves now exist for all R. However the speed and the amplitude of the fastest waves are clearly well below all other predictions, which suggests that the re-summation procedure leads to an overestimation of the strength of the saturating nonlinearities.

All other models we have considered include more than one equation. Many have a structure analogous to that of the oldest one, namely Shkadov's model (2, 3) involving h and the local flow rate q and obtained by a simple averaging of the boundary-layer equations [23]. Solitary waves it produces have properties summarized by Curves 3. While it is known to overestimate the value of the instability threshold for non-vertical planes, *i.e.* to underestimate the linear instability mechanism, at the nonlinear stage, the comparison with other models shows that it also notably delays the value at which the speed and the height of the waves increases rapidly. Equations (19) in [24], are very similar to our simplified Galerkin model including dispersive viscous terms, but with slightly different coefficients and additional terms of higher order in the surface tension contribution. We do not show the properties of the solitary waves generated by this model since they are not much different from those of Shkadov's model, except for the fact that the additional surface-tension terms introduces an artificial singularity forbidding the existence of solutions with large gradients, so that the curve stops at $R \simeq 4$ in the conditions considered.

Applying a center manifold reduction technique, Roberts [27] was able to obtain a two-equation model by eliminating all damped velocity modes except the first one. Originally cast in terms of h and $\bar{u} = \frac{1}{h}\int_0^h u\,{\rm d}y$, this model can be rewritten for h and q, specifically equation (14) in reference [27]. It displays a structure similar to our simplified Galerkin model, with coefficients also rather close to ours. The differences in the coefficients of the terms we have in common come from the fact that he used trigonometric basis functions instead of polynomials, which might be questionable since sines and cosines are eigenmodes of the free-surface linearized problem around the rest state and not around the basic semi-parabolic profile. Some of the additional terms present in his formulation could possibly be recovered by performing an adiabatic elimination of s_1 and s_2 from our full second-order model. We do not display the results corresponding to his model because

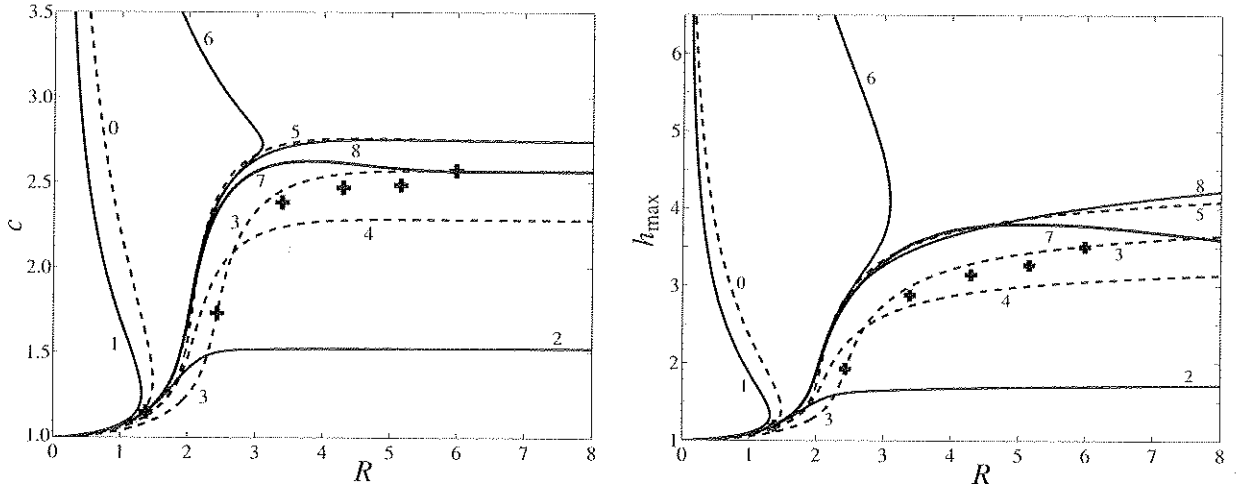

Fig. 2. Speed (left) and amplitude (right) of one-hump solitary waves as functions of the Reynolds number for the different models considered. The plane is vertical and the Kapitza number is $\Gamma = 252$: curves 0: Benney's equation (dashed); curves 1: second-order Benney's equation (solid); curves 2: Ooshida's equation (solid); curves 3: Shkadov's model (dashed); curves 4: first-order model of [29] (dashed); curves 5: first-order Galerkin model (dashed); curves 6: second order model of [29] (solid); curves 7: full second-order Galerkin model (solid, thicker); curves 8: simplified second-order Galerkin model (solid). "plus" signs: two-dimensional first-order boundary layer equations [8].

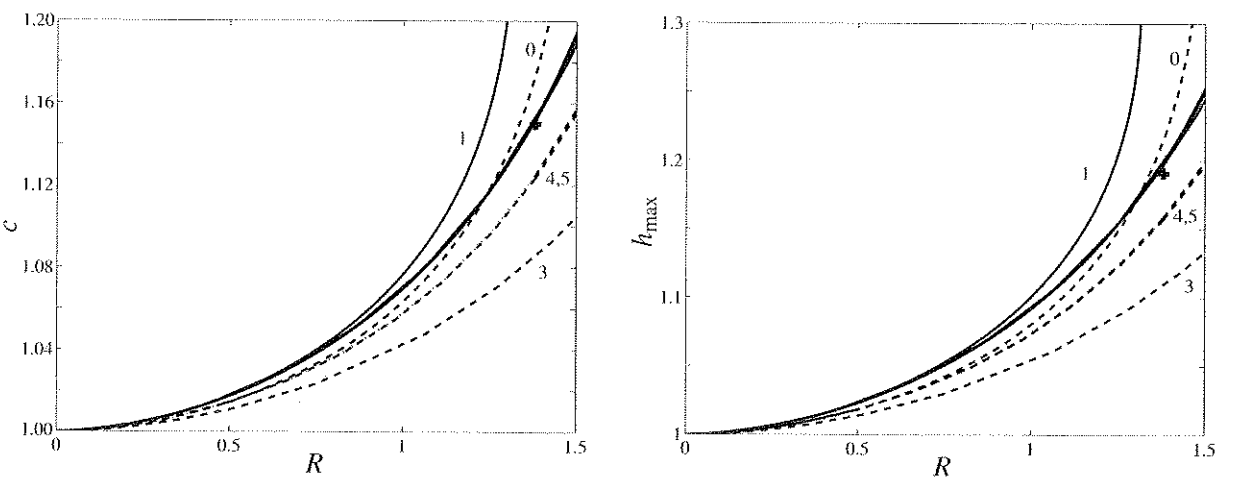

Fig. 3. Low Reynolds number close up of Figure 2, see corresponding caption.

they are practically indistinguishable from ours using the full second-order model up to about $R = 2.5$. Then they grow more slowly while high-order derivatives of h become unrealistically large so that above $R \approx 3.5$ we lose confidence in the obtained results. This behavior could be connected to the presence of the additional terms alluded to above and possibly be cured by some regularization "technique à la" Ooshida [21].

Let us now turn to our models. Results from the models developed in this paper are displayed as Curves 5 (first-order, Eqs. (11, 26)), Curves 7 (full, second-order, Eqs. (11, 38–40)) and Curves 8 (simplified, second-order, Eqs. (11, 41)), those from models in our previous paper [29] as Curves 4 (first-order) and Curves 6 (second order). From the consideration of Curves 4 that corresponds to equation (58) in [29], completed by the mass conservation equation (11), one understands that the goals of correcting the deficiency of Benney's equation and improving the behavior of Shkadov's model close to threshold have been achieved: while solitary waves exist for all R, their speed and their amplitude now increase at the right place. However they seem to be somewhat underestimated at large R. This model was obtained by an integral-collocation method and the same strategy was used for the second-order model leading to Curves 6. Whereas excellent agreement with all other second-order formulations is observed up to $R \sim 3$, the Curves turns back there, signaling a loss of the solution and the companion possibility of finite-time singularities that were observed in the simulations for certain flow regimes. This phenomenon has to be related to the poor convergence properties of the method [30]. Discrepancies between Curves 5 (first-order) and 7 (full second-order) become obvious only when the amplitude and the speed of the waves are large. Curves 8 stand for the simplified second-order Galerkin model and remain very close

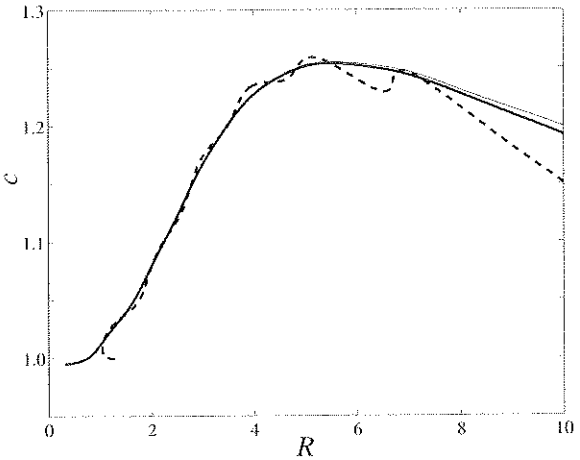

Fig. 4. Wave speed as a function of the Reynolds number for periodic wave-train solutions with $\alpha = 0.07$, $W = 76.4$ and average thickness $\langle h \rangle = h_N$. The thick solid line is the prediction of full second-order model, the thin line corresponds to simplified second-order model and the dashed line is the prediction of the first-order model.

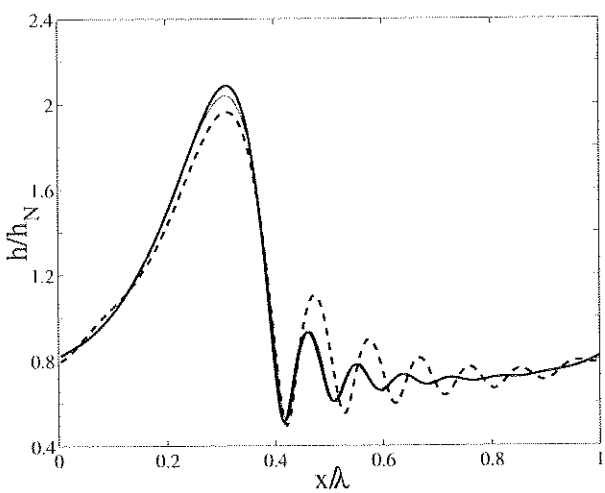

Fig. 5. Wave profiles corresponding to $R = 10$ and the same other conditions as in Figure 4, see corresponding caption.

to Curves 5. This suggests that, as far as the celerity and maximum height of the waves are concerned, the differences between the first-order model and the simplified second-order models are minor, which might be due to the fact that they both resolve the flow with a single polynomial (however, see below for more subtle differences attributed to viscous dispersion effects). Inertial terms contribute only to the full second-order model. This might be an explanation of the discrepancy between results from the full and the simplified models but one must keep in mind that the former resolves the flow field on three polynomials instead of one and that the corrections to the parabolic profile, measured by s_1 and s_2, are liable to play an important role.

In Figures 2 and 3 we have added some results ("plus" signs) of calculations performed by Chang *et al.* using the two-dimensional first-order boundary layer equations (12–15) and given in Table 1 of [20]. Whereas close to onset we observe good agreement with all models (except Shkadov's, which does not treat it properly), divergences appear at larger R. The waves' characteristics have the right order of magnitude but we do not know how to explain the discrepancies (if they are significant at all) for the computational approaches are very different.

A second test is obtained from the properties of long-wavelength periodic wave-trains. We have determined the wave's velocity c as a function of the Reynolds R number at given wavevector α (Fig. 4) or reciprocally of α at given R (Fig. 6), and studied the waves' profiles (Fig. 5). These special solutions approaching homoclinicity are computed by means of a pseudo-spectral method combined with an Euler-Newton continuation scheme [38] using up to 256 complex Fourier modes. Periodic boundary conditions are taken at a distance $\lambda = 2\pi/\alpha$ where α is the chosen wavevector. We assume that plane is vertical ($B = 0$) and that the thickness of the film averaged over one wavelength $\langle h \rangle$ is kept fixed and equal to h_N as derived from $R = \frac{1}{3}h_N^3$. Figures 4 and 5 displays our results for $\alpha = 0.07$ and a Weber number $W = 76.4$, in view of a comparison with DNS results in [6] (see Fig. 11 there).

The speed of these wave-trains is given as a function of the Reynolds number in Figure 4. Solutions of the full and simplified second-order Galerkin models both bifurcate from the basic state on the neutral stability curve at $R \approx 0.32$ with $c \approx 0.995$ in good agreement with DNS results. Differences between the predictions of the two models become noticeable only for large amplitude waves. For the first-order model (11, 26), the same family of waves builds up at $R \approx 1.26$ with $c = 1$ and the corresponding curve displays wrinkles very similar to those obtained with the first-order boundary layer equations by Chang *et al.* [8].

The waves' profiles obtained from our three models for $R = 10$ are given in Figure 5. Whereas the curves corresponding to the two second-order models are practically indistinguishable, ahead of the hump the profile obtained with the first-order model exhibit running capillary ripples of much larger amplitude. This corroborates the experimental observations showing that Shkadov's model (2, 3), a first-order approximation, overestimates the amplitude of the ripples (see *e.g.* Fig. 8.26 in [2]). This is also in agreement with the corresponding numerical findings in Figures 16 and 18 of [6].

Not unexpectedly, the strong difference between the results obtained with the simplified second-order model and the first-order model can obviously be attributed to the omission of the viscous dispersion terms in the latter. By contrast, inertial effects contributing to the difference between the two second-order models seem of smaller importance, at least for the properties and in the range of Reynolds numbers considered.

The computations of Salamon *et al.* have also shown that drastically different bifurcation scenarios take place when viscous dispersion effects are modified [6]). It is indeed well-known that in the case of the Kuramoto-Sivashinsky equation (KS) traveling wave solutions

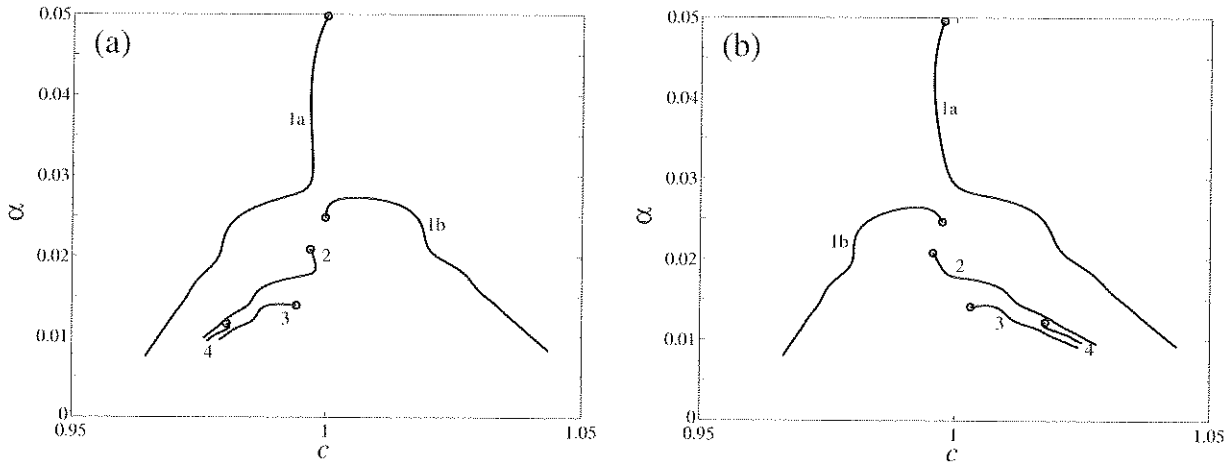

Fig. 6. Speed c of periodic wave-trains as a function of their wavevector α for $R = 2.066$, $\Gamma = 3375$, $B = 0$ (vertical plane) and fixed averaged thickness $\langle h \rangle = h_{\rm N}$ (conditions chosen to fit those of [6]) (a) first-order model; (b) simplified second-order Galerkin model.

bifurcate from a standing wave through a pitchfork bifurcation and that the bifurcation becomes imperfect when dispersion is added [39]. In our case, the bifurcation diagram associated to this phenomenon is displayed as Curves 1a, and 1b in velocity-wavenumber plots of Figure 6. In agreement with the DNS results of [6] (see Figs. 12 and 14 there), we see that the picture is drastically changed when viscous dispersion effects are taken into account, *i.e.* when we pass from first (a) to second order (b). Indeed, in the first case with no viscous dispersion, Branch 1a connects the primary solutions to slow waves ($c < 1$) whereas Branch 1b corresponds to fast waves ($c > 1$) and in the second case the reverse situation holds when viscous dispersion effects are taken into account. Similar results using our previous second-order model derived in [29] have been presented elsewhere [40]. The other curves labelled as 2, 3, 4 in Figures 6a and 6b correspond to different solutions approaching, at small wavevectors, various types of solitary waves having several humps behind the front ripples and bifurcating from subharmonics of the primary solution. They are shown here in view of a comparison with the findings of Salamon *et al.* [41].

Finally, our approach giving direct access to the flow rate q, we can equally chose to prescribe the average film thickness $\langle h \rangle$ or the average flow rate $\langle q \rangle$. This possibility allowed us to compare our findings with experiments performed at controlled flow rate. Table 1 displays the wave speeds computed from our modeling, to those derived from several DNSs and laboratory experiments, with either $\langle h \rangle = h_{\rm N}$ or $\langle q \rangle = q_{\rm N} = \frac{1}{3} h_{\rm N}^3$, when appropriate. Satisfactory agreement is again obtained in all cases.

To conclude, the realistic modeling of film flows is an important step towards the understanding of the growth of space-time disorder in free-surface open flows. In the two-dimensional case, our systematic strategy has led to three more and more complex models, which, as far as the properties of solitary waves are concerned, yield results that are in general agreement with previous investigations.

Table 1. Comparison between wave speeds (cm/s) from the experimental work of Kapitza and Kapitza, from DNSs and from the present modelling. Parameters are $R = 6.07$, $W = 76.4$ (mean flow rate $\langle q \rangle = 0.123$ cm^2/s, surface tension $\sigma/\rho = 29$ cm^3/s^2, wavelength $\lambda = 1.77$ cm).

	$\langle h \rangle = h_{\rm N}$	$\langle q \rangle = q_N$
Eqs. (11, 38–40)	23.5	20.4
Eqs. (11, 41)	23.5	20.3
Eqs. (11, 26)	23.2	20.5
Kapitza & Kapitza [10]	–	19.5
Ho & Patera [42]	24.7	–
Salamon *et al.* [6]	23.5	–
Ramaswamy *et al.* [7]	23.1	–

The inter-comparison of our models further points out the role of viscous dispersion (first-order model compared to the simplified second-order model) and that of the inertial terms and a finer description of the velocity field (comparison of the full and simplified second-order models).

Studying more closely the full second-order model, one can show by linearization of (38–40) that the relaxation time of the fluctuations of the flow rate $\tilde{q}$ around the value forced by the local thickness (*i.e.* by setting $\tilde{q} = q - \frac{1}{3} h^3$) is more than one order of magnitude larger than the relaxations times of s_1 and s_2 that describe the corrections to the semi-parabolic basic velocity profile. According to the theory of dynamical systems, the latter variables are fast and therefore slaved to the slow variables, here h and q. This property should be used to eliminate them adiabatically, which would yield a model in terms of h and q only, but with more complicated effective nonlinearities. Pushing the argument, one can notice that only h is neutral at the long wavelength limit and that q should also be eliminated, yielding an effective "surface equation". However the argument is only asymptotic and, as is often the case, the corresponding series has no good convergence properties. This ends with solutions having singular behavior at too large Reynolds numbers. The regularization

of the series has proven its merits but apparently leads to an overestimation of the nonlinear saturating corrections. We believe that in the range of intermediate Reynolds numbers considered, the future is with models involving h and q only. Such models should be more accurate than Shkadov's model, more complete than our own first-order models, past [29] or present (only the latter is consistent at first order in the gradient expansion within the framework of weighted residual methods resting on polynomial), and extending our simplified second-order model. This extension could derive from a reduction of our full second-order model by an adiabatic elimination of irrelevant fields at which we now work. As we showed, our strategy is not limited to the modelling of two-dimensional flows and the extension to three dimensions is relatively straightforward. The detailed study of curved solitary waves, secondary instabilities towards three-dimensional patterns and irregular waves in view of a comparison with experimental observation will thus now be our major concern.

This work has been supported by a grant from the Délégation Générale à l'Armement (DGA) of the French Ministry of Defense. Ch. R.-Q. would like to thank C. Jones and M. Romeo for providing him with references [36] as well as the AUTO97 and HOMCONT softwares.

References

1. H.-C. Chang, Annu. Rev. Fluid Mech. **26**, 103 (1994).
2. S.V. Alekseenko, V.E. Nakoryakov, B.G. Pokusaev, *Wave flow in liquid films* (Begell House, New York, 1994).
3. P. Huerre, *Open shear flow instabilities*, in *Developments in fluid mechanics: a collection for the millennium*, edited by G.K. Batchelor, H.K. Moffat, M.G. Worster (Cambridge Univ. Press, Cambridge, to appear).
4. M.C. Cross, P.C. Hohenberg, Rev. Mod. Phys. **65**, 851 (1993).
5. (a) J. Liu, J.D. Paul, J.P. Gollub, J. Fluid Mech. **250**, 69 (1993); (b) J. Liu, J.P. Gollub, Phys. Fluids **6**, 1702 (1994); (c) J. Liu, B. Schneider, J.P. Gollub, Phys. Fluids **7**, 55 (1995).
6. T.R. Salamon, R.C. Armstrong, R.A. Brown, Phys. Fluids **6**, 2202 (1994).
7. B. Ramaswamy, S. Chippada, S.W. Joo, J. Fluid Mech. **325**, 163 (1996).
8. H.C. Chang, E.A. Demekhin, D.I. Kopelevitch, J. Fluid Mech. **250**, 433 (1993).
9. (a) V.G. Levich, *Physico-chemical hydrodynamics* (Fizmatgiz, Moscow, 1959); (b) E.A. Demekhin, I.A. Demekhin, V.Y. Shkadov, Izv. Ak. Nauk SSSR, Mekh. Zhi. Gaza No. 4, 9 (1983) [transl. Fluid Dynamics **4** (Plenum Publ., 1984), pp. 500–506].
10. P.L. Kapitza, S.P. Kapitza, Zh. Ekper. Teor. Fiz. **19**, 105 (1949); Also in *Collected papers of P.L. Kapitza*, edited by D. Ter Haar (Pergamon, Oxford), pp. 690–709.
11. J. Benney, J. Math. Phys. **45**, 150 (1966).
12. B. Gjevik, Phys. Fluids **13**, 1918 (1970).
13. S.P. Lin, J. Fluid Mech. **63**, 417 (1974).
14. H. Haken, *Synergetics*, 3rd edn. (Springer-Verlag, New York, 1983).
15. A. Pumir, P. Manneville, Y. Pomeau, J. Fluid Mech. **135**, 27 (1983).
16. Y. Kuramoto, T. Tsuzuki, Prog. Theor. Phys. **55**, 536 (1976); G.I. Sivashinsky, Acta Astronautica **4**, 356 (1977); Y. Kuramoto, Prog. Theor. Phys. Suppl. **64**, 1177 (1978).
17. O.Y. Tsvelodub, Izv. Ak. Nauk SSR, Mekh. Zh. Gaza **4**, 142 (1980).
18. H.C. Chang, Phys. Fluids **29**, 3142 (1986).
19. S.W. Joo, S.H. Davis, S.G. Bankoff, Phys. Fluids. A **3**, 231 (1991).
20. H.C. Chang, E.A. Demekhin, E. Kalaidin, AIChE J. **42**, 1553 (1996).
21. T. Ooshida, Phys. Fluids **11**, 3247 (1999).
22. B.A. Finlayson, *The method of weighted residuals and variational principles, with application in fluid mechanics, heat and mass transfer* (Academic Press, 1972).
23. V.Ya. Shkadov, Izv. Ak. Nauk SSSR, Mekh. Zhi. Gaza No. 2, 43 (1967) [transl. Fluid Dynamics **2** (Faraday Press, New York, 1970), pp. 29–34].
24. T. Prokopiou, M. Cheng, H.C. Chang, J. Fluid Mech. **222**, 665 (1991).
25. L.-Q. Yu, F.K. Wasden, A.E. Dukler, V. Balakotaiah, Phys. Fluids **7**, 1886 (1995).
26. J.-J. Lee, C.C. Mei, J. Fluid Mech. **307**, 191 (1996).
27. A.J. Roberts, Phys. Lett. A **212**, 63 (1996).
28. E.A. Demekhin, M.A. Kaplan, V. Ya. Shkadov, Izv. Ak. Nauk SSSR, Mekh. Zhi. Gaza No. 6, 73 (1987) (transl. Fluid Dynamics **6** (Plenum Publ., 1988) pp. 885–893.
29. Ch. Ruyer-Quil, P. Manneville, Eur. Phys. J. B **6**, 277 (1998).
30. Ch. Ruyer-Quil, P. Manneville, "Convergence of weighted-residual methods applied to the modeling of film flows down inclined planes" in preparation.
31. Ch. Ruyer-Quil, Ph.D. thesis, École Polytechnique, 1999.
32. H. Schlichting, *Boundary-layer theory* (McGraw-Hill, 1955).
33. The procedure should thus more properly be called a *tau-method*; see, *e.g.* D. Gottlieb, S.A. Orszag, *Numerical analysis of spectral methods* (SIAM, Philadelphia, 1977).
34. R.E. Kelly, D.A. Goussis, S.P. Lin, F.K. Hsu, Phys. Fluids A **1**, 819 (1989).
35. Ch. Ruyer-Quil, P. Manneville, *Secondary instabilities of falling films using models*, at *Interfaces for the Twenty-First Century*, Monterey, CA, 08/16–19/1999, and in preparation.
36. (a) E.J. Doedel, H.B. Keller, J.P. Kernévez, Int. J. Bif. Chaos **1**, 493 (1991); (b) E.J. Doedel, H.B. Keller, J.P. Kernévez, Int. J. Bif. Chaos **1**, 745 (1991); (c) A.R. Champneys, Y.A. Kuznetsov, Int. J. Bif. Chaos **4**, 785 (1994).
37. H.C. Chang, E.A. Demekhin, E. Kalaidin, J. Fluid Mech. **294**, 123 (1995).
38. E.L. Allgower, K. Georg, *Numerical continuation methods* (Springer-Verlag, 1990).
39. H.C. Chang, E.A. Demekhin, D.I Kopelevitch, Physica D **63**, 299 (1993).
40. C. Ruyer-Quil, P. Manneville, in *Advances in Turbulence VII*, edited by U. Frisch (Kluwer, 1998), pp. 93-96.
41. For the simplified second-order model (Fig. 6b), curve 1a starts at $\alpha = 0.0496$ and curve 1b branches off at $\alpha = 0.0247$. Subsequent solutions set in at $\alpha = 0.0208$, 0.0141 and 0.0123 in close agreement with the values given in [6].
42. L.W. Ho, A.T. Patera, Comp. Meth. Appl. Mech. Eng. **80**, 355 (1990).